Supplementary Materials

Supplementary Figures

Fig. S1. (A) Distribution of 84 study sites within the “Whittaker biomes” defined by mean annual temperature and precipitation. Shading of each dot indicates the magnitude of change in peak NDVI from 1986-2020. **(B)** Distribution of study sites by continent, with the shading of each dot indicating whether the long-term trend in NDVI was significantly positive or negative, or non-significant (see also Fig. 1).

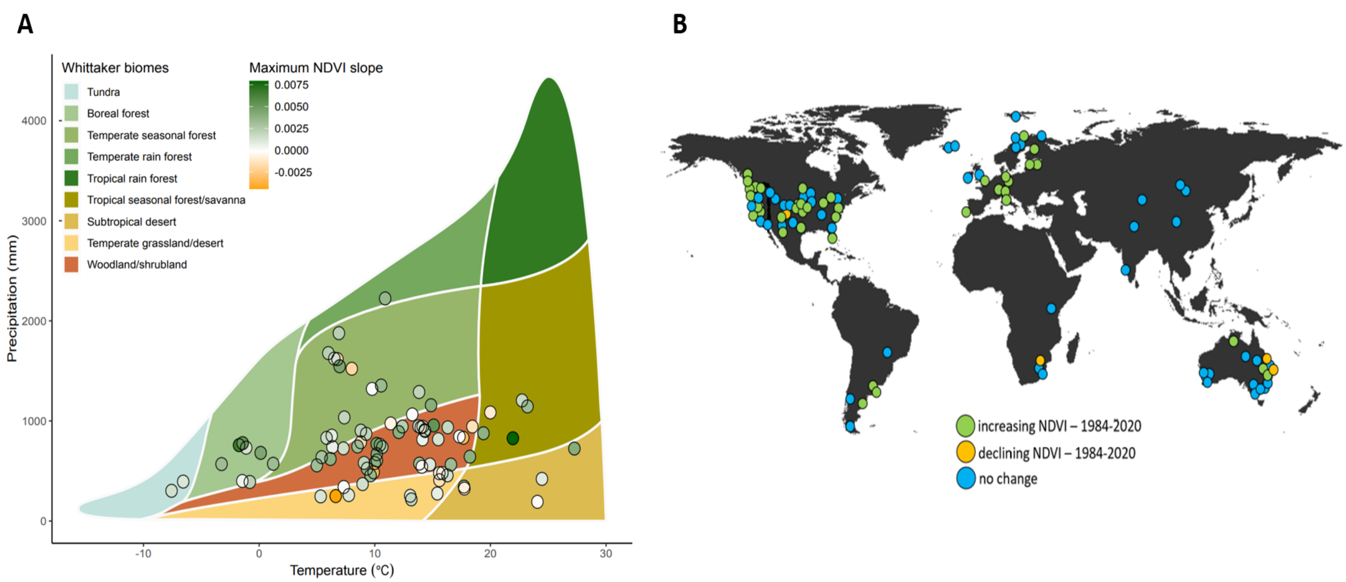

Fig. S2. Factors associated with changing peak NDVI by continent. Principle components for the factors driving changes in peak NDVI, with increasing NDVI most closely associated with longer growing seasons, increases in temperature and precipitation and high species richness per site. Sites with declining NDVI were most pronounced in arid sites of Australia, Asia, and South America. Loading matrices, significance tests for the component axes, and factor correlations are presented in Fig. S3.

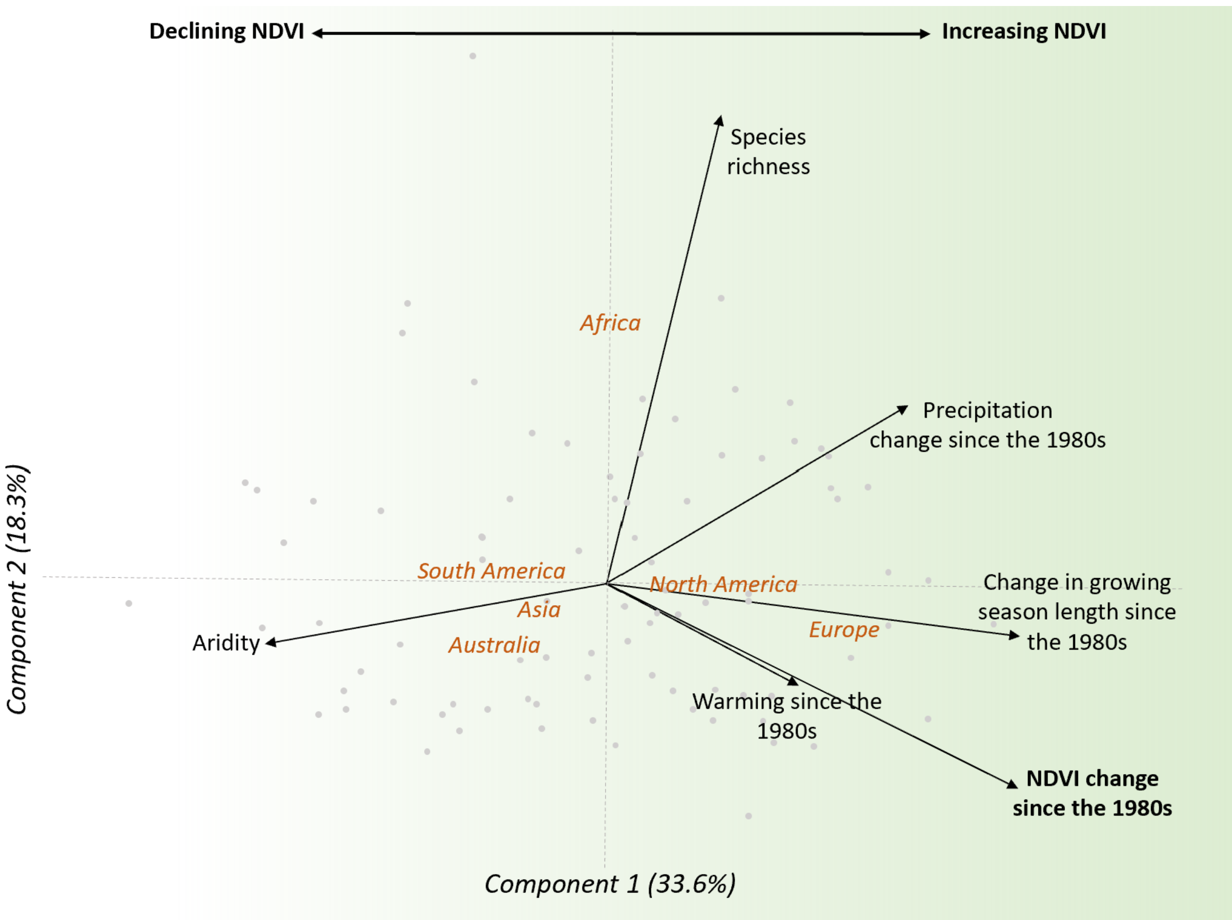

Fig. S3. Principle components details for Figure S2, showing alignment of changing NDVI with major factors identified by model simplification. (A) Only the 1st axis was significant (Bartlett's test) relating to (B) significant positive (red) associations among shifts in maximum NDVI, temperature, precipitation, and growing season and negative (blue) association with aridity. Loadings for axis 1 positively associated with European sites including Arctic locations, and negatively associated with arid sites in Asia, Australia, and South America. Loadings for axis 2 are shaped in large part by the African sites (e.g., Serengeti grasslands) having the largest levels of species richness.

A

Axis	Eigenvalue	% explained	Cumulative %	Chi-square	DF	p
1	2.018	34	34	56.1	14.8	**<0.0001**
2	1.097	18	52	11.9	11.9	0.06
3	0.967	16	68	8.0	8.01	0.08
4	0.819	13	81	4.7	4.7	0.10

B

Factor	Principle Axis 1	Principle Axis 2
Species richness	0.2100	0.88365
Growing Season length	0.7556	0.1077
Aridity	-0.6169	0.1848
Change in temperature	0.35908	0.1888
Change in precipitation	0.55897	0.32813
Change in NDVI	0.76237	-0.38425
Continent		
Africa	0.0154	1.787
Asia	-0.551	0.1077
Australia	-1.421	-05298
Europe	1.2123	0.1949
North America	0.078	0.0684
South America	-0.4141	0.0551

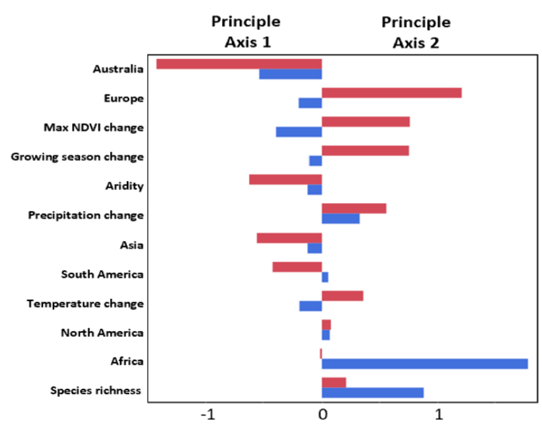

Fig. S4. Lack of overall global phenological trend (linear regression; $F_{1,83} = 0.95$, $p = 0.33$) in the site-specific relationship between changes (slope of the temporal trend starting from 1986) in start-of-season emergence, and the onset of end-of-season senescence. Our highest latitude site (Svalbard, Norway) was an extreme outlier and thus excluded from the analysis.

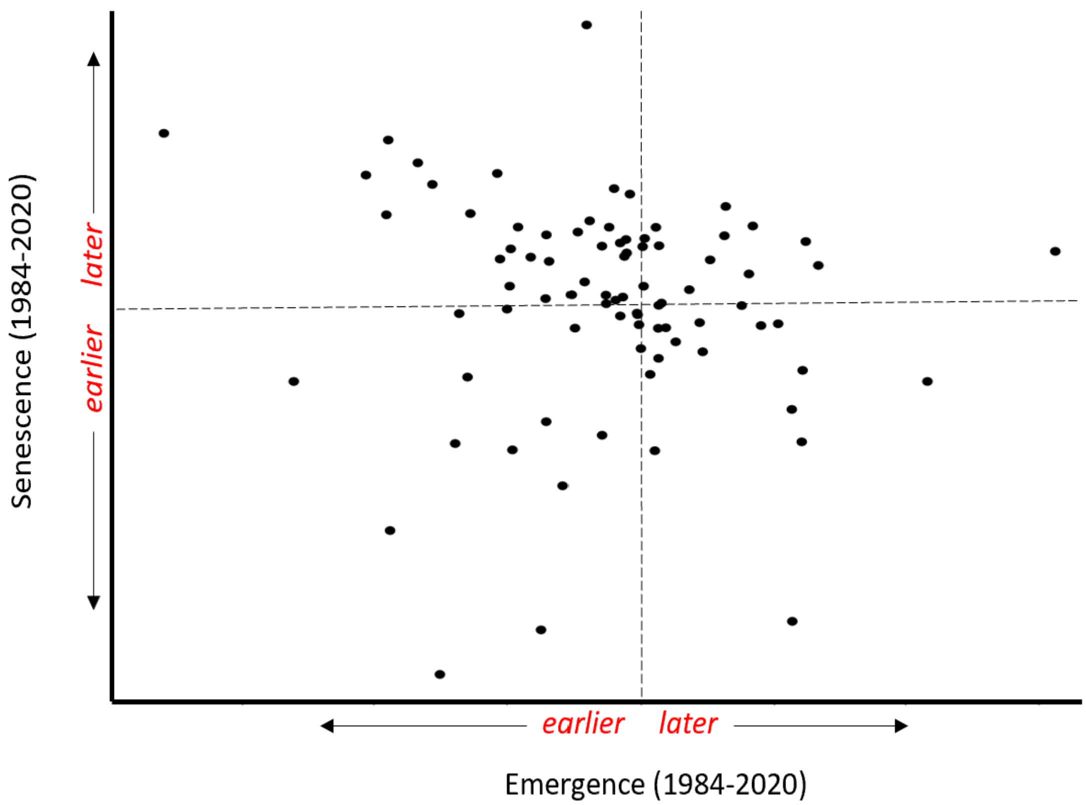

Fig. S5. Relationship between the slopes of annual warming and precipitation change since the mid-1980s. All sites have a positive slope in temperature change (i.e., all sites are warming), whereas only 49% of sites are getting wetter. The sites that have become the driest since 1986 (based on reductions in annual precipitation) come from both the Northern and Southern Hemispheres, occurring in California and Australia respectively. Although warmer air can sometimes be associated with wetter conditions (e.g., greater snowfall in a warming Arctic), we do not see this as a global trend given that many sites are warming but getting drier.

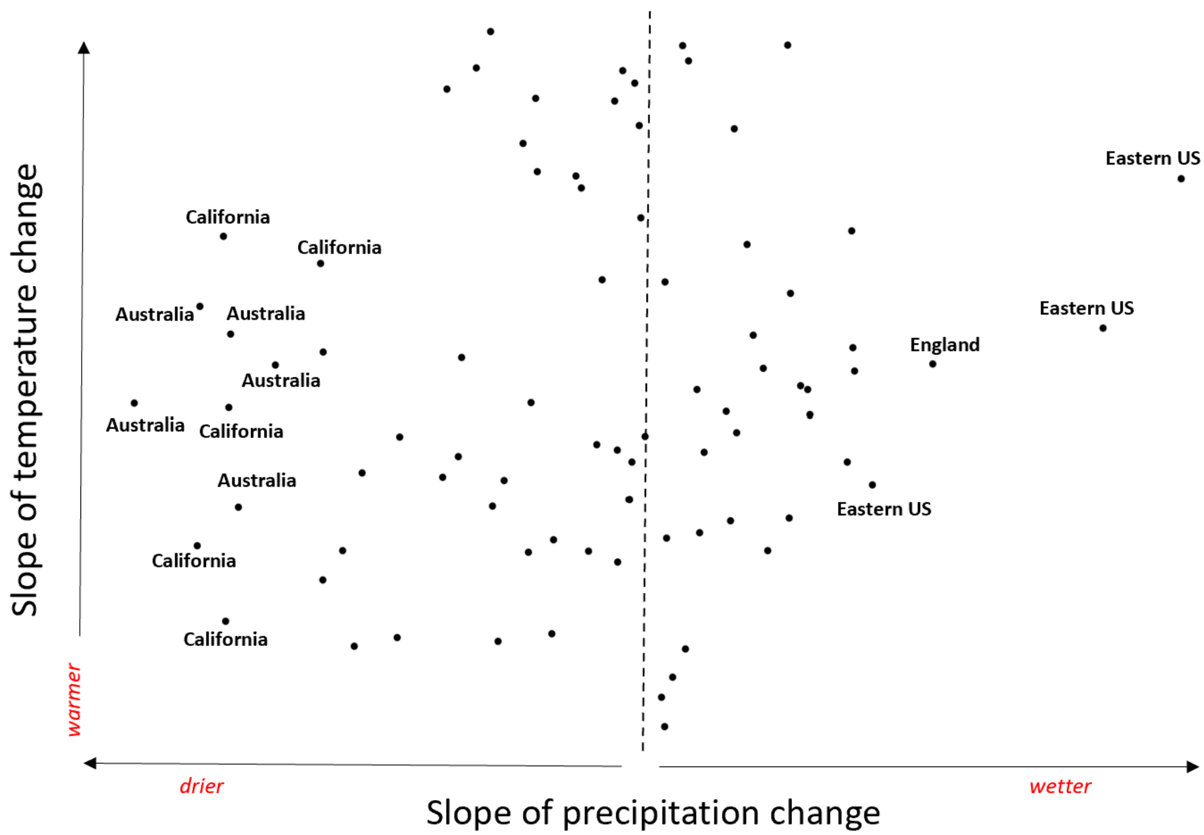

Fig. S6. **Trends in annual warming from 1986-2020 for global grasslands**, by (A) mean annual temperature with the greatest rates of increase in areas with the coldest baseline MATs (e.g., European Arctic and montane steppe grasslands of Asia; $F_{1,83}$= 16.2, p <0.0001) and by (B) latitude with the greatest rates of increase in the Northern Hemisphere (logged fit: $F_{1,83}$= 38.7, p <0.0001). Fitted lines derived from linear regression.

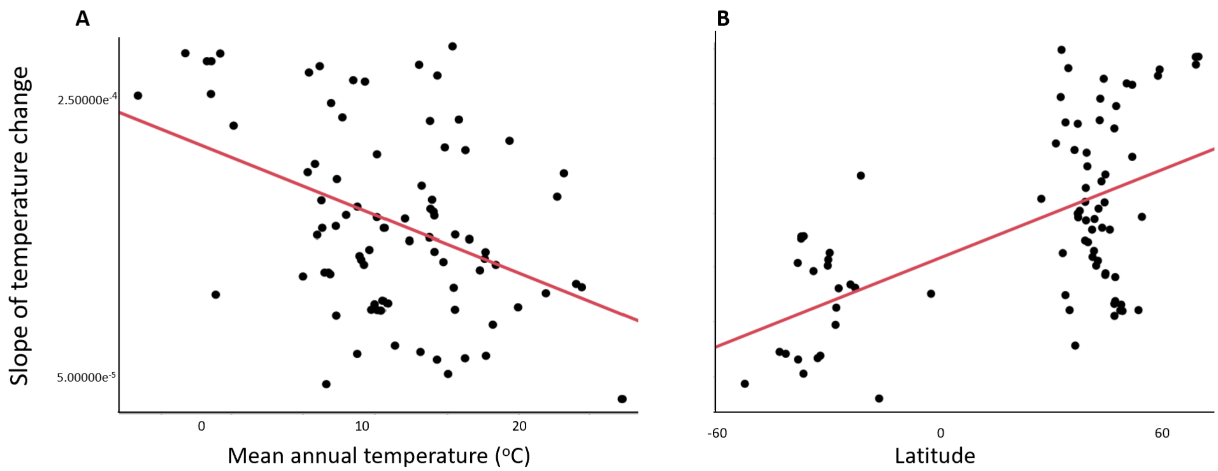

Fig. S7. Relationship between the slope of changing site-level NDVI (decreasing [yellow] or increasing [green], and two factors relating to potential evapotranspiration (PET): slope of the change in site level PET from 1986-2020 (left) and the baseline aridity index by site based on the ratio between annual precipitation to annual PET (right). Relationships were tested with linear regression, with trend line only shown for the significant fit (right). Sites with precipitation<PET are classified as "arid grasslands" and sites with precipitation>PET are classified as "mesic grasslands". There was no relationship between changes in PET and changes in site-level NDVI ($F_{1,83} = 0.21$, $p = 0.64$). In contrast, baseline levels of aridity were able to predict changes in NDVI ($F_{1,83} = 7.04$, $p = 0.0096$), with the sites receiving more annual precipitation having the highest increases in NDVI. In total 59 of our 84 sites were arid, but less than 50% of these showed negative temporal trend lines in NDVI over time (right panel). That is to say, not all arid sites had NDVI declines.

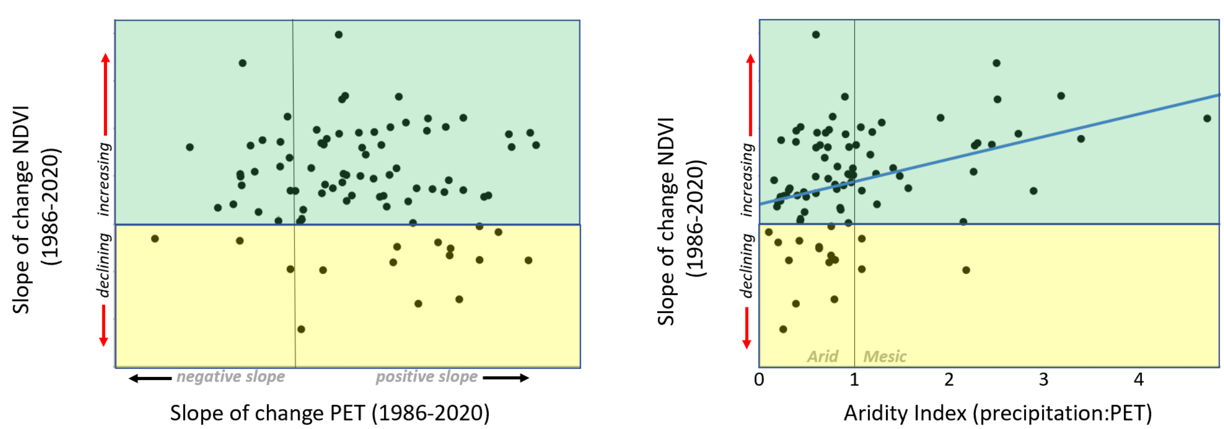

Fig. S8. **Trends in spring warming by latitude for global grasslands**. There was no overall trend by latitude based on linear regression ($F_{1,83}$=0.15; p = 0.69), but the range of vernal temperature shifts was wider in the Northern Hemisphere including 14 sites showing cooling.

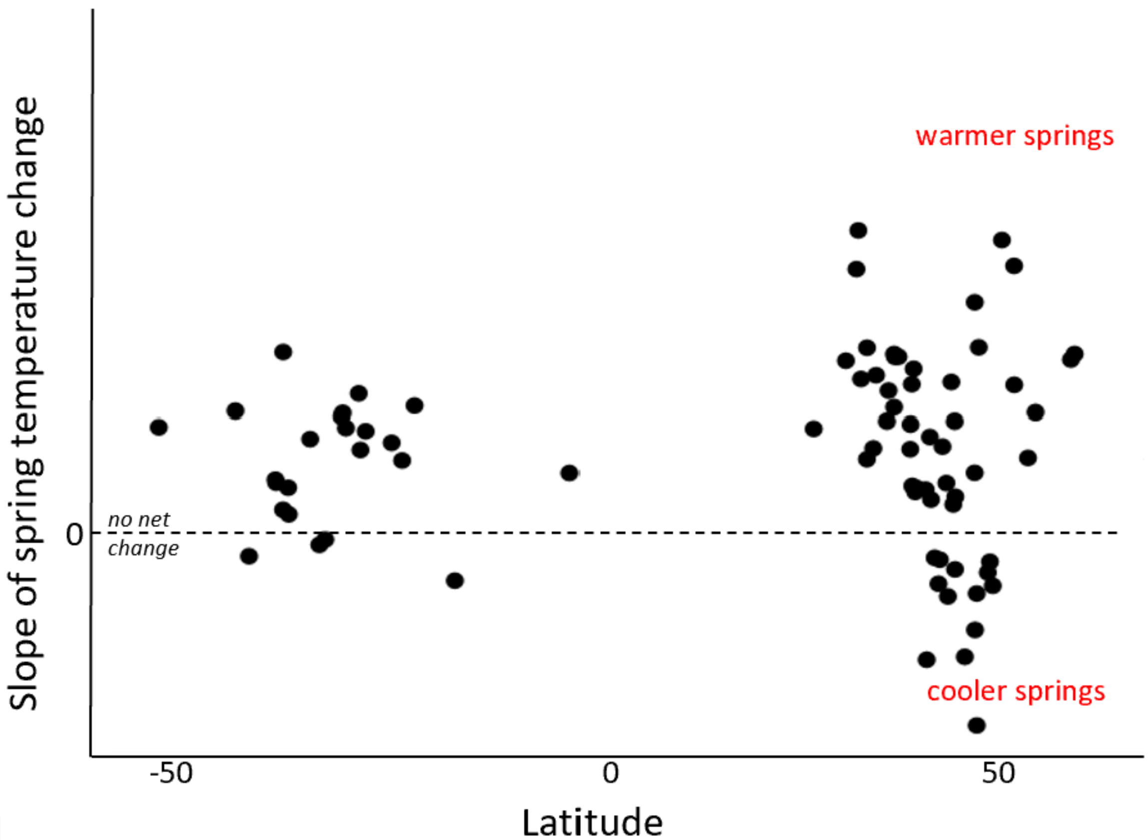

Fig. S9. Testing of relative explanatory power of major factors influencing change in NDVI as shown in Table 1, using “effect leverage plots” that allow the two-dimensional linear X-Y depiction of multi-factor higher-order statistical interactions. These leverage plots depict the influence of adding an explanatory factor to the model, given the other factors already in the model. As shown in Table 1 and Fig. 2, most of the influence on NDVI change derives from changes in Growing Season Length (the slope of GSL [“GSL_slope”]) and its interaction with warming since the 1980s (“OverallTemp_slope”). The influence of species richness is significant when interacting with growing season length and warming, compared to its effect alone (see also Fig. 2). “Logworth” are -log transformations of each factor’s p-value, which illustrates the degree of difference in importance between the model factors.

Source	Logworth	PValue
GSL_slope	8.905	0.00000
GSL_slope*OverallTemp_slope	3.647	0.00023
OverallTemp_slope	1.773	0.01685
Richness*GSL_slope	1.463	0.03442
Richness*OverallTemp_slope	0.799	0.15901
Richness	0.569	0.26987
Richness*GSL_slope*OverallTemp_slope	0.023	0.94755

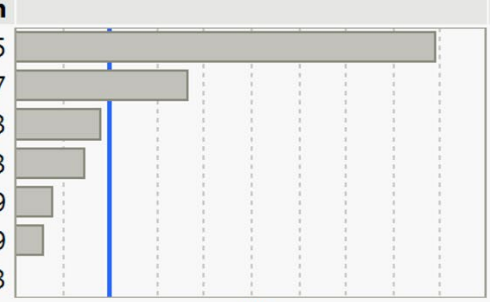

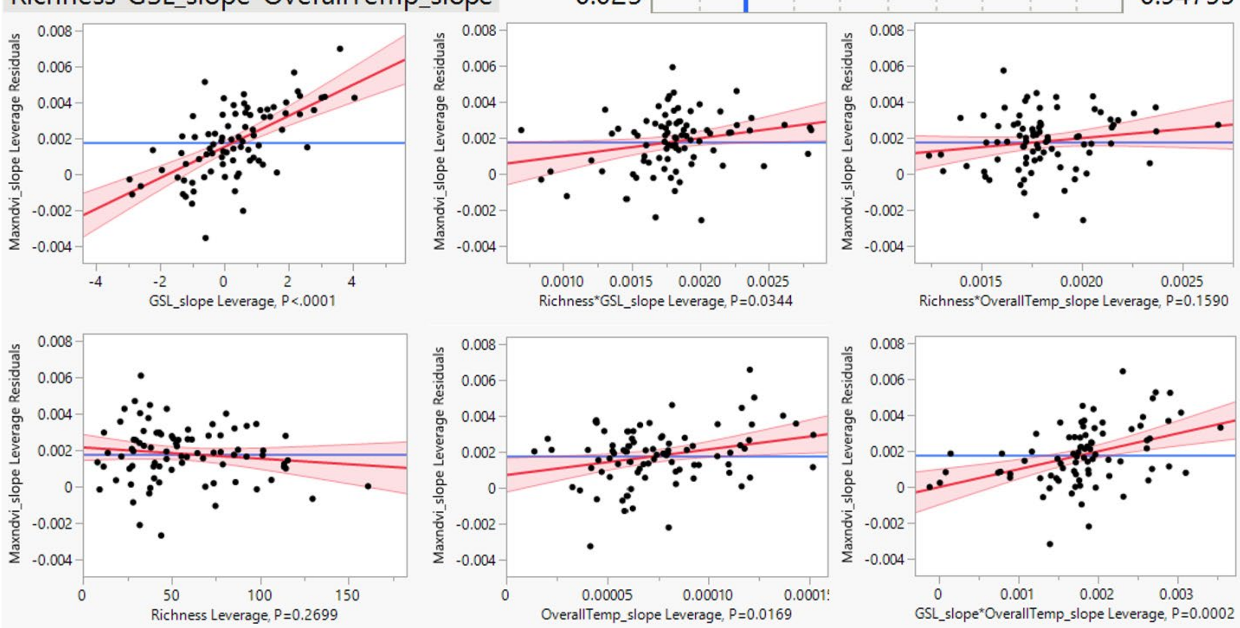

Fig. S10. Relationship between year of observation and (left) harvested live peak biomass plot^{-1} and (right) estimated peak biomass based on NDVI. Data are pooled for all sites globally. Live peak biomass derives from sites with three or more years of harvest, and are the same data used to test the NDVI-based estimates of live aboveground peak biomass (Fig 4). These data demonstrate a significant increase in plot-level biomass with time ($F_{1,545}$=4.1; p=0.04). NDVI data also demonstrate a significant increase among sites over time ($F_{1,442}$=15.1; p<0.0001). Shaded areas are the confidence curves for the fitted trend lines, based on best-fit linear regressions. Error bars on 1 SE +-.

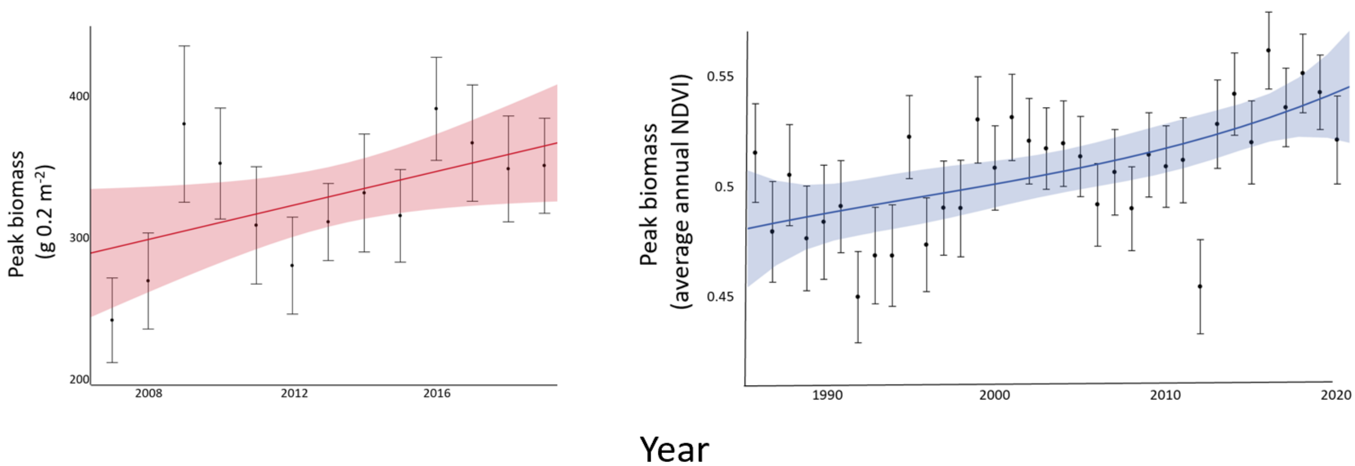

Fig. S11. Frequency distribution of major abiotic and biotic factors among the 84 sites.

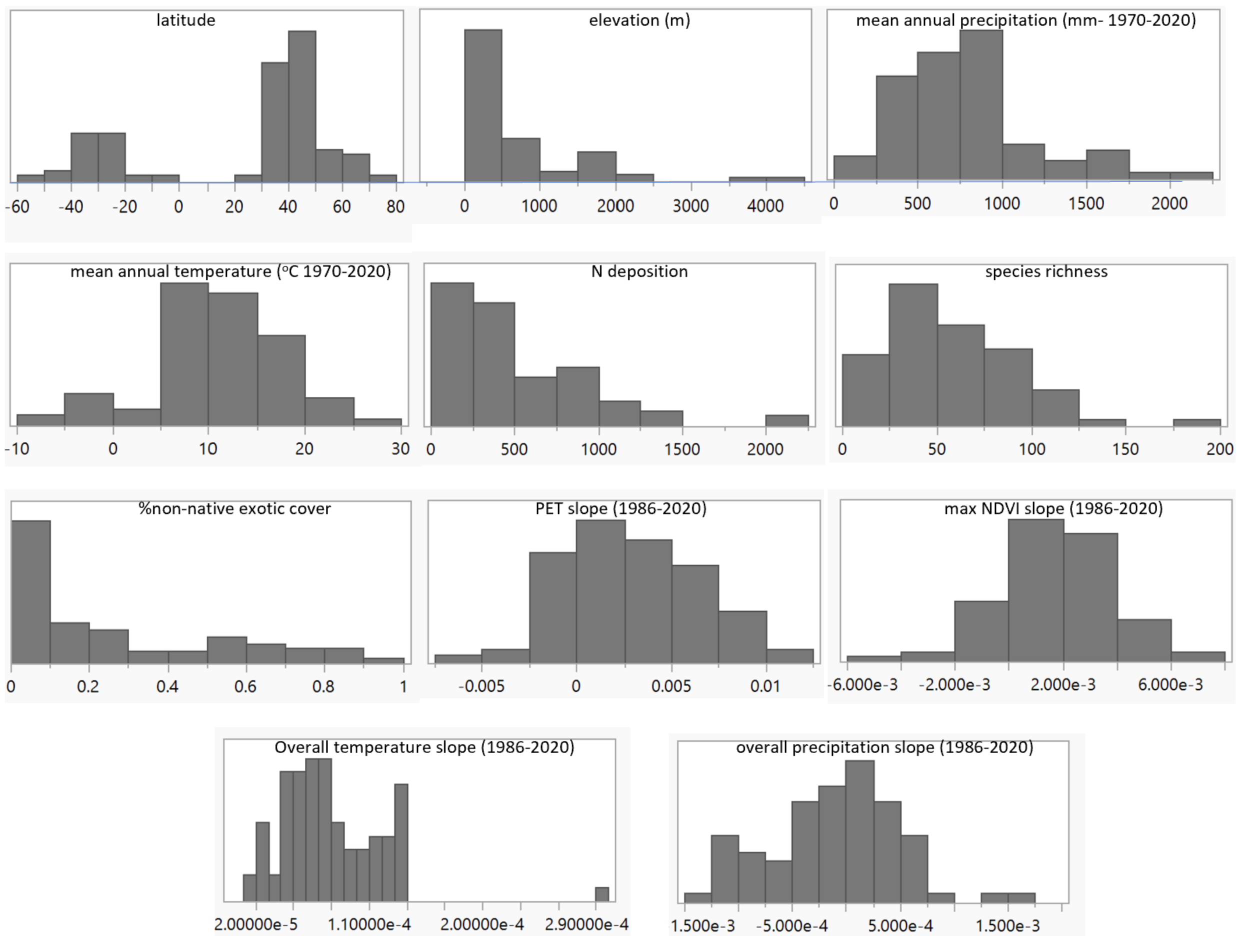

Fig. S12. Depiction of a Nutnet site viewed from Google Earth, where the locations of the 5 x 5 m plots can be easily seen. We located our 30 m circular NDVI plot at least 50 m away from the Nutnet plots to ensure that they did not overlap with the Nutnet treatments or with changes in vegetation such as tree canopy cover. The 30 m circular plot was used to collect all remotely sensed data starting no earlier than 1986 and extending to 2020 (depending on the site). The locations of both areas were non-randomly positioned in grassland that was homogenous in plant cover, topography, and soil type. The NDVI plot location was determined visually/manually using the satellite images, with consultation with each site principal investigator. The circular plot was placed close enough to represent the same grassland community as the Nutnet plots, but far enough away to avoid any disturbance that might be associated with Nutnet data collection (e.g., trampling damage). We used plot-specific spatial coordinates measured with a hand-held GPS (red star) to test potential locational errors (easting and northing) that can occur with Google Earth coordinates (blue star). Photo source: Google Earth

Fig S13. Depiction of NDVI data for a typical site (here, from central California) for 1982-2020. Because data were typically unavailable or sparse for 1982-1985, we only used data starting in 1986 at this site. Trends lines are the individual year-site combination splines, from which the fitted NDVI values (red, green, and blue dots) were extracted. The open circles are the actual NDVI readings, and the black line is the fitted NDVI spline from which phenological dates were extracted. Values below green-up and senescence are winter 'trough' periods.

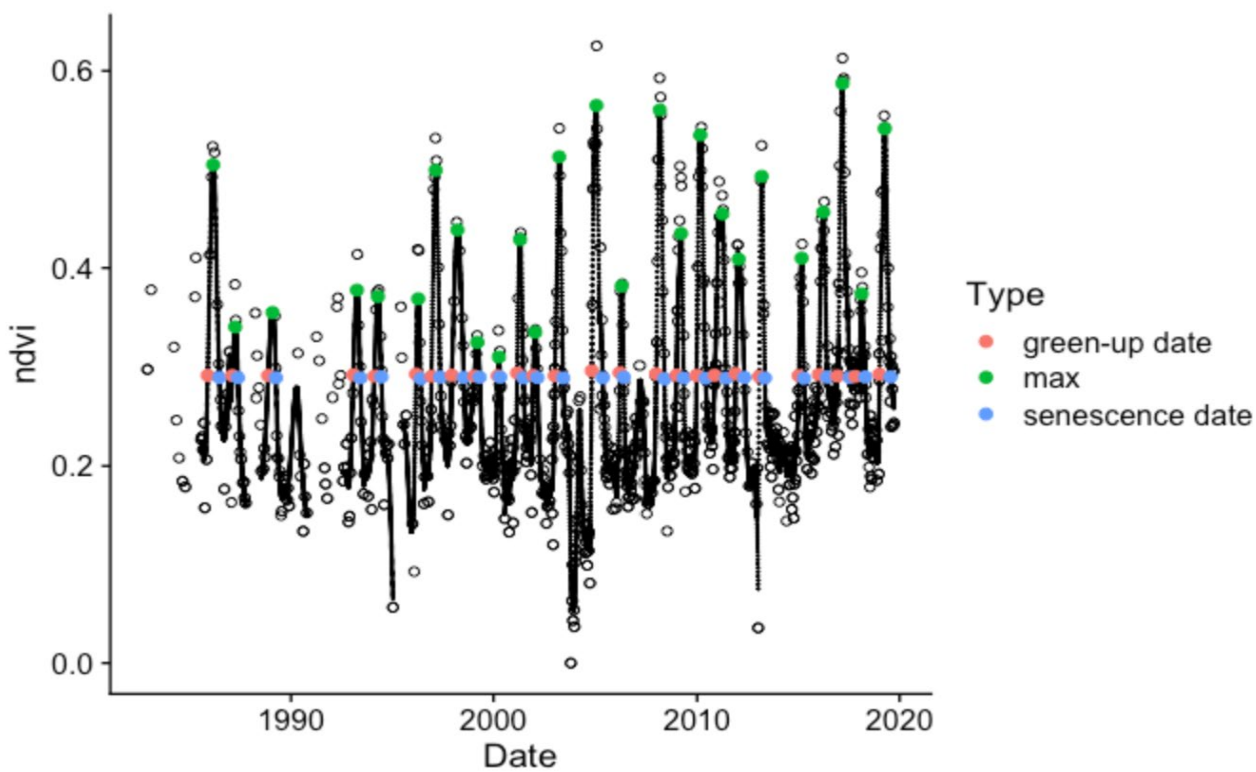

Supplementary Tables

Table S1: List of sites used in the study, sorted by latitude (Lat) and including elevation above sea level (Elev), mean annual precipitation (1970-2020) (MAP), mean annual temperature (1970-2020) (MAT), the number of species per site ("species richness") including the mean percentage (0-100%) of non-native exotic species, and whether the site is arid (PET>annual precipitation) or mesic (PET<precipitation). Two sites*** were excluded from the main analysis due to extreme outliers (see Supplemental Methods for details). Additional site information can be found at www.nutnet.org

Site code	Continent	Lat	Elev (m)	MAP (mm)	MAT (ºC)	Species richness	% exotic	Aridity
potrok	South America	-51.9	150	249	6.6	34	0	arid
spv	South America	-42.6	70	216	13.1	22	30	arid
bari	South America	-41.0	786	787	8.7	40	50	arid
derr	Australia	-37.8	38	565	14.7	19	50	arid
marc	South America	-37.7	6	907	14.3	65	26	arid
bogong	Australia	-36.8	1760	1678	5.9	42	10	arid
nilla	Australia	-36.8	280	947	13.7	24	65	arid
chilcas	South America	-36.2	15	955	15.0	99	24	arid
kiny	Australia	-36.2	90	408	15.5	114	51	arid
yarra	Australia	-33.6	19	844	17.3	31	68	arid
ping	Australia	-32.4	338	456	16.2	23	77	arid
mtca	Australia	-31.7	285	324	17.7	67	33	arid
summ	Africa	-29.8	679	944	18.4	105	0	arid
ukul	Africa	-29.6	843	832	17.6	176	6	arid
gilb	Africa	-29.2	1748	943	14.1	74	0	arid
burrawan	Australia	-27.7	425	643	18.2	43	23	arid

pinj	Australia	-27.5	38	1085	19.9	34	77	arid
bunya	Australia	-26.8	0	817	15.4	17	17	arid
ethamc	Australia	-23.7	104	192	24.0	45	9	arid
mitch	Australia	-22.4	242	421	24.4	17	0	arid
lagoas	South America	-20.9	279	1145	23.2	33	21	mesic
kidman	Australia	-16.1	87	724	27.2	30	10	arid
sereng	Africa	-2.2	1536	827	21.9	75	0	arid
arch	North America	27.1	8.2	1205	22.7	80	1	arid
temple	North America	31.0	184	877	19.3	105	5	arid
kibber	Asia	32.3	4241	400	-1.4	37	0	arid
jorn	North America	32.5	1342	275	15.4	35	0	arid
elliot	North America	32.8	200	344	17.7	51	50	arid
azitwo	Asia	33.5	3500	733	-1.1	71	0	arid
lubb	North America	33.6	977	480	15.8	19	11	arid
sevi	North America	34.3	1600	252	13.0	79	2	arid
sedg	North America	34.7	550	478	15.5	34	54	arid
unc	North America	36.0	141	1157	14.8	67	30	mesic
hast	North America	36.2	750	975	11.3	32	46	mesic
hall	North America	36.8	194	1289	13.8	53	26	mesic
ucsc	North America	36.8	140	542	14.0	17	81	arid
elkh	North America	36.9	50	815	14.1	22	80	arid
jasp	North America	37.4	120	574	13.8	34	8	arid
comp	Europe	38.8	200	564	16.5	97	1	arid
mcla	North America	38.8	642	936	13.9	78	52	arid
hopl	North America	39.0	598	1065	13.2	126	5	arid
konz	North America	39.0	440	889	12.0	97	3	arid
sier	North America	39.2	197	936	16.3	123	50	arid
sage	North America	39.4	1920	831	5.8	45	0	arid
bnbt	North America	39.5	240	944	12.3	44	18	arid
bldr***	North America	39.9	1633	487	9.9	49	70	arid

doane	North America	40.6	418	739	10.6	41	17	arid
sgs	North America	40.8	1650	369	8.9	78	11	arid
cdpt	North America	41.2	965	456	9.6	84	11	arid
glcr	North America	41.3	343	771	10.1	28	19	arid
cbgb	North America	41.7	275	871	9.2	98	27	arid
barta	North America	42.2	767	581	9.0	55	4	arid
kbs	North America	42.4	288	903	8.7	79	63	arid
hart	North America	42.7	1508	259	7.7	48	14	arid
bynb	Asia	42.8	2470	394	-6.5	17	0	arid
uwo	North America	43.1	325	1035	7.3	33	66	mesic
lake	North America	43.3	452	726	7.2	89	25	arid
gall	Europe	43.7	34	900	14.3	53	0	arid
koffler	North America	44.0	301	853	6.2	51	49	mesic
bnch	North America	44.2	1318	1618	6.7	51	9	mesic
bttr	North America	44.2	1500	1623	6.4	66	9	mesic
look	North America	44.2	1500	1877	6.8	51	8	mesic
shps	North America	44.2	910	246	5.3	97	18	arid
cdcr	North America	45.4	270	740	6.3	123	22	arid
lead	North America	46.6	2	2224	10.8	13	0	mesic
msla	North America	46.6	1169	340	7.3	51	27	arid
valm	Europe	46.6	2320	681	0.1	115	0	mesic
glac	North America	46.8	33	1354	10.5	17	65	mesic
msum	North America	46.8	311	556	4.9	33	7	arid
frue	Europe	47.1	995	1546	6.9	40	12	mesic
smith	North America	48.2	62	605	10.1	57	82	mesic
amcamp	North America	48.4	41	580	10.0	26	70	mesic
cowi	North America	48.8	50	762	10.4	26	92	mesic
bayr	Europe	49.9	340	745	8.5	70	5	arid
badlau	Europe	51.3	120	523	9.3	67	6	arid
hero	Europe	51.4	60	668	10.1	57	4	mesic

burren	Europe	53.0	112	1320	9.7	82	0	mesic
lancaster	Europe	53.9	180	1522	8.0	34	0	mesic
elva	Europe	58.2	63.5	638	5.4	51	0	mesic
kirik	Europe	58.7	7.5	620	6.1	84	0	mesic
thth***	Europe	65.9	380	572	1.2	58	0	mesic
abisko	Europe	68.3	410	390	-0.8	19	0	mesic
kark	Europe	68.3	730	758	-1.7	35	0	mesic
vass	Europe	68.4	608	778	-1.4	39	0	mesic
kilp	Europe	69.0	700	569	-3.2	101	0	mesic
sval	Europe	78.7	50	302	-7.5	14	0	mesic

Table S2: Model output testing factors associated with grazing. List of top factors detected in association with changing peak NDVI, among 46 grasslands globally with installed grazing exclosures (see Methods). Factors including the slope of the change in growing season length (GSL), the slope of the change in temperature (Temperature), slope of the change in precipitation (Precipitation), and levels of nitrogen deposition (N) by site 2014-2016 (N). Grazing refers to log response ratios between biomass inside exclosures versus outside exclosures at each of 46 sites where exclosures were constructed. Parameter estimates and standard errors refer to standardized input variables. Model values are weighted regressions using the inverse of the standard error of the slopes, (i.e. slopes with smaller standard error get a bigger weight, with lower standard error a smaller weight – e.g. Seabloom et al.[78]).

Factor	Estimate	Standard Error	Z value	p
Intercept	**0.0016**	**0.0002**	**7.34**	**<0.001**
GSL	**0.0024**	**0.0005**	**4.80**	**<0.001**
GSL*Temperature	-0.0007	0.00011	0.65	0.51
N	0.0003	0.0005	0.57	0.57
Elevation	-0.0003	0.0006	0.54	0.59
Grazing*Precipitation	-0.0005	0.0012	0.42	0.67
% Exotic Plant Richness	-0.0002	0.0005	0.42	0.68
Precipitation	-0.0002	0.0006	0.41	0.68
Temperature	0.0001	0.0003	0.40	0.69
Aridity*Temperature	-0.0003	0.0009	0.38	0.70
Aridity	-0.0001	0.0002	0.25	0.82

GSL*Species Richness	0.0002	0.0007	0.23	0.82
Temperature*Species Richness	0.00001	0.0005	0.23	0.82
Species Richness	0.00000	0.0002	0.05	0.96
Grazing	0.00000	0.0002	0.01	0.99

Table S3: Analysis of community-level trait indices on shifts in maximum NDVI. None are significantly associated with shifting site-level biomass, despite these traits being generally associated with the production of aboveground plant biomass (e.g., specific leaf area (SLA), Leaf N and P, and plant height. FD = functional diversity and CWM = community weighted mean, following van der Plas et al. 2020[37]. These traits measures are non-temporal composite values, derived from the site-level species lists at each site. Those lists derived from 30 randomly located 1 m^2 plots per site.

Term	Estimate	Std Error	T ratio	Prob > t
Leaf P (FD)	0.002	0.001	1.8	0.07
Leaf C (CWM)	0.00003	0.00003	1.2	0.25
SLA (CWM)	0.00009	0.00008	1.1	0.3
Height (FD)	0.0006	0.001	0.5	0.6
Leaf P (CWM)	0.0002	0.0008	0.2	0.8
Leaf C (FD)	0.0003	0.002	0.2	0.9
Leaf N (FD)	-0.001	0.001	-0.12	0.9
Height (CWM)	-0.0009	0.002	-0.5	0.63
Leaf N (CWM)	-0.0001	0.000009	-1.1	0.28
SLA (FD)	-0.02	0.001	-1.7	0.1

Table S4. Model output for residual analysis, testing factors associated with estimation bias between remote-sensed NDVI and field-measured live aboveground biomass (Fig. 4). “Latitude” is the cosine of latitude, as this more accurately represents the curvature of Earth’s surface. For this entire model, the multiple R-squared = 0.67 ($F_{4,53}$=26.81, p <0.0001). The residual analysis strictly for NDVI with live biomass, with no additional factors had a smaller R^2 of 0.52. The residual analysis for NDVI with live biomass, with the addition of latitude and elevation (without species richness) increased the R^2 to 0.63 (an increase in accuracy of 21%). Adding species richness, as shown here, had a smaller increase in precision, increasing the R^2 from 0.63 to 0.67.

Factor	Estimate	Standard Error	t value	p
(intercept)	3.31	0.58	5.74	<0.0001
NDVI	3.1	0.38	8.23	<0.0001
Latitude	0.58	0.2	3.02	0.004
Elevation	-0.11	0.04	-2.82	0.007
Species richness	0.28	0.11	2.5	0.015

Table S5: List of 8 sites used in the study, sorted by latitude (Lat) and including relative accuracy, implemented as root mean square error (RMSE), between the positions of the plot centers logged from the handheld GPS and from Google Earth Pro imagery (Fig. S10). RMSE was calculated as the geodesic distance errors between the latitudes ($RMSE_{Lat}$), the longitudes ($RMSE_{Lon}$), and the combined horizontal errors at 95% confidence ($RMSE_{95}$).

Site code	Continent	Lat	$RMSE_{LAT}$	$RMSE_{LON}$	$RMSE_{95}$
mcla	North America	38.8	1.25	0.71	2.82
hopl	North America	39	0.81	0.37	1.75
bnch	North America	44.2	0.43	0.45	1.23
msum	North America	46.8	0.6	2.41	4.87
hero	Europe	51.4	0.45	0.17	0.95
nap	North America	50.4	2.58	2.74	7.38
lac	North America	50.8	2.01	0.84	4.26
kilp	Europe	69	0.74	0.55	1.8

The georeferencing accuracy of Google Earth Pro imagery is variable and not reported by Google so we used the GPS logs of plot centers as reference points for calculating agreement between the plot positions from both data sources as follows:

In this equation:

$$RMSE_y = \sqrt{\frac{1}{n}\sum_{i=1}^{n}(y_i - \hat{y}_i)^2}$$

RMSE is the root mean square error

n is the number of observations

y_i is the GPS Latitude

y_i-hat is the Google Earth Pro Latitude

This equation calculates the square of the difference between the observed and predicted values, sums these squared differences, divides by the number of observations, and then takes the square root. The result is the RMSE between the latitude values for plot centers.

In this equation:

$$RMSE_x = \sqrt{\frac{1}{n}\sum_{i=1}^{n}(x_i - \hat{x}_i)^2}$$

RMSE is the root mean square error

n is the number of observations

x_i is the GPS Longitude

$x_{i\text{-hat}}$ is the Google Earth Pro Longitude

The RMSE values for latitude and longitude are combined by calculating the square root of each squared quantity. The result is multiplied by 1.96 for 95% confidence of the relative accuracy between the GPS and Google Earth Pro positions of the plot centers.

$$RMSE_{yx} = 1.96 \times \sqrt{RMSE_y{}^2 + RMSE_x{}^2}$$

For the subset of sites we evaluated for relative accuracy, the horizontal displacement is less than the georeferencing error of Landsat imagery. It is also less than the buffer between the nutnet plots and the Landsat plots.

All plot positions in Google Earth Pro were logged as placemarks and exported in keyhole markup format then converted to a geopackage to store all points. The GPS logs were stored as a comma separated values (csv) file. The geopackage and csv file were loaded into a Jupyter notebook for analysis and processed according to the code in GitHub.